CENPU promotes tumorigenesis and stem cell properties in triple-negative breast cancer by suppressing lysosomal furin degradation

SHUJUAN SUN[1,2], ZHENYU HOU[3], LING QIANG[1] and DONGDONG ZHOU[1]

[1]Shandong Provincial Key Laboratory of Precision Oncology, Shandong Cancer Hospital and Institute, Shandong First Medical University and Shandong Academy of Medical Sciences, Jinan, Shandong 250117, P.R. China; [2]Key Laboratory of Cancer Prevention and Intervention, China National Ministry of Education, The Second Affiliated Hospital, Zhejiang University School of Medicine, Hangzhou, Zhejiang 310058, P.R. China; [3]Department of Gastrointestinal Surgery, Qilu Hospital, Jinan, Shandong 250012, P.R. China

Received December 12, 2024; Accepted July 21, 2025

DOI: 10.3892/ijmm.2025.5649

Abstract. Centromere protein U (CENPU), a critical component of the kinetochore complex, structurally integrates with spindle microtubules to mediate chromosome segregation during mitosis. However, the association between CENPU expression levels and tumors is largely unknown. Immunohistochemistry and western blotting were used to analyze CENPU expression and prognostic value in breast cancer tissues. CENPU overexpressing/knockdown cell lines were constructed for 4D-data-independent acquisition quantitative proteomics and enrichment analyses. Functional assays, including flow cytometry, mammosphere formation, wound healing and Transwell assay, were used to assess the effects of CENPU on breast cancer stemness, migration and invasion. The associations among CENPU, nerve growth factor (NGF), proNGF and furin were also explored through western blotting, co-immunoprecipitation and ELISA experiments. Finally, xenograft mouse models were established to verify the *in vivo* effects of CENPU on tumorigenesis and the inhibitory effect of furin inhibitor on CENPU-promoted tumor growth. In the present study, immunohistochemistry and western blotting assessment of human breast cancer tissue specimens revealed a positive association between CENPU expression and the degree of invasiveness. The aforementioned functional analyses demonstrated that CENPU promoted stem cell-like behavior and tumorigenicity, and induced malignancy in BC cells. Mechanistically, western blotting analysis demonstrated that CENPU promoted furin activity by inhibiting its lysosomal degradation. Furin, which is a precursor-processing enzyme of (NGF), promoted the conversion of NGF precursor to NGF, which could promote BC stem cell properties in triple-negative BC (TNBC). A tumorigenesis assay conducted in xenograft mouse models showed that CENPU promoted tumorigenesis, and treatment with a furin inhibitor suppressed this effect. The findings of the present study revealed that CENPU serves a critical role in furin-mediated signaling responsible for tumorigenesis. Therefore, CENPU may be a novel molecular target in TNBC.

Correspondence to: Dr Dongdong Zhou, Shandong Provincial Key Laboratory of Precision Oncology, Shandong Cancer Hospital and Institute, Shandong First Medical University and Shandong Academy of Medical Sciences, 440 Jiyan Road, Jinan, Shandong 250117, P.R. China
E-mail: wasabi1214@163.com

Key words: centromere protein U, furin, nerve growth factor precursor, nerve growth factor, tumorigenesis

Introduction

Triple-negative breast cancer (TNBC) is a distinct BC subtype characterized by the absence of estrogen receptor, progesterone receptor and human epidermal growth factor receptor 2 expression, along with unique molecular expression characteristics (such as frequent mutations in *TP53* and *PIK3CA*, and dysregulation of MYC, EGFR and Wnt/β-catenin pathways), biological behavior (such as early visceral metastasis and 'metastatic burst' within 3 years post-diagnosis) and clinicopathological features (such as higher histological grade, stromal tumor-infiltrating lymphocytes and poorer 5-year survival) (1). TNBC exhibits a high rate of distant metastasis (liver: 34.5%; brain: 9.8%; lung: 32.4%), high odds of visceral and brain metastases, rapid progression (3-year distant metastasis-free rate: 57.9% vs. 85.2% in luminal A; 1-year recurrence rate after surgery: 18.4%), and limited treatment options (2-6). Understanding the molecular basis of TNBC occurrence and progression and identifying efficient therapeutic targets are key issues in TNBC treatment that warrant urgent attention.

BC stem cells (BCSCs) are tumor-initiating cells that can self-renew and are highly tumorigenic. An increasing amount of studies suggest that cancer stem cells promote tumorigenesis, metastasis, recurrence and drug resistance as well as are the major source for heterogeneity of cancer cells (7-9). In 2003, Al-Hajj *et al* (10) purified BCSCs from BC patient samples for the first time and showed that tumor stem cells, even in limited quantities, induced tumorigenesis in immunodeficient mice. At

present, strategies for identifying BCSCs are primarily based on two key biological characteristics of BCSCs, namely their self-renewal ability and their differentiation ability, which enable them to evade the effects of most cytotoxic chemotherapeutic drugs (11). BCSCs also frequently exhibit high levels of drug efflux and a superior metabolic capacity. This makes them more likely to survive chemotherapy than non-BCSCs, which leads to tumor recurrence and metastasis (12,13). Therefore, combined treatment with cancer stem cell antagonists and conventional cancer treatment tools is a promising therapeutic approach for reducing BC recurrence and metastasis.

The centromere protein U (*CENPU*) gene, located on chromosome 4q35.1, participates in mitosis as an important part of the centromere complex (14). In our previous study, it was demonstrated that CENPU promoted angiogenesis in TNBC by suppressing the ubiquitin-related degradation of cyclooxygenase-2 (15). In non-small cell lung cancer, CENPU enhances the proliferative, migratory and invasive potential of cells by activating the Wnt/β-catenin pathway (16). However, the mechanisms underlying the effects of CENPU on BC formation are not well-documented.

Nerve growth factor (NGF) is an important neurotrophic factor involved in the regulation of cell differentiation and target neuron survival. Both NGF and NGF precursor protein (proNGF) are biologically active, but the two proteins may have contrasting biological functions (17-20). The maturation of proNGF to NGF requires cleavage by furin precursor protein-processing enzymes (21,22).

Furin is the earliest discovered mammalian precursor protein-processing enzyme and is primarily responsible for the cleavage of functional proteins in an organism (23). Excessive or aberrant cleavage by furin is associated with diseases, such as cancer (24). The shearing action of furin on proNGF contributes to the paradoxical biological function of its downstream receptors that activate different pathways depending on the form of its ligand. Unprocessed proNGF exerts its apoptosis-promoting effects by binding to low-affinity p75 neurotrophin receptor. By contrast, furin-processed NGF mediates survival in tumor cells through high-affinity binding to the tropomyosin receptor kinase A proto-oncogene receptor, which interacts with and phosphorylates STAT3 to enhance gene transcription and promote BCSC properties in TNBC and HER2-enriched BC (20,25).

The study of BCSCs and their role in tumor progression is crucial for developing novel therapeutic strategies. The objective of the present study was to investigate the expression of CENPU in different types of breast lesions and its potential role in BCSC self-renewal, tumorigenesis and the invasive behavior of BC cells. Understanding the mechanisms underlying CENPU function could provide insights into the molecular pathways that drive BC aggression and metastasis. To achieve these aims, a combination of immunohistochemistry, functional assays and mechanistic studies was employed to explore the expression patterns and functional significance of CENPU in BC cell lines.

Materials and methods

Cell culture and treatment. Human MDA-MB-231 (TNBC) and T47D (BC) cells were acquired from the American Type Culture Collection. Cal51 (TNBC) cells were acquired from the German Collection of Microorganisms and Cell Cultures GmbH. Cell culture was performed as previously described (15). Specifically, Cal51 was cultured in 15% DMEM/F12 medium, MDA-MB-231 in 10% DMEM high-glucose medium, and T47D (luminal) in 10% RPMI-1640 medium (Gibco; Thermo Fisher Scientific, Inc.). All the media were supplemented with 10% FBS (cat. no. 04-001-1ACS; Biological Industries; Sartorius AG) and 1% penicillin-streptomycin (cat. no. P1400; Beijing Solarbio Science & Technology Co., Ltd.). The cells were maintained in a humidified incubator at 37˚C with 5% CO_2 and sub-cultured at 75-85% confluence. Cycloheximide (CHX; cat. no. HY-12320) (20 μM) was purchased from MedChemExpress. MG132 (cat. no. Y210207) (10 μM) and chloroquine (CQ; cat. no. Y210184) (100 μM) were purchased from Beyotime Institute of Biotechnology. Cell treatments were performed at 37˚C for 12 h. NGF-neutralizing antibody (cat. no. ALM-006-250UG; Thermo Fisher Scientific, Inc.) was used at a final concentration of 1 μg/ml in complete culture medium at 37˚C for 24 h before subsequent assays.

Immunoblotting. MDA-MB-231, T47D and Cal51 cells were lysed with RIPA lysis buffer (Beyotime Institute of Biotechnology) supplemented with 1% PMSF. Cellular proteins were quantified using a BCA Assay kit (MilliporeSigma). Equal volumes of total protein (30 μg) were resolved using 10% SDS-PAGE and electro-transferred onto PVDF membranes (MilliporeSigma), and the membranes were blocked with 5% non-fat milk for 1 h at room temperature. Next, the membranes were incubated with primary antibodies overnight at 4˚C. The primary antibodies used were as follows: CENPU (1:1,000; cat. no. YN1585; Immunoway Biotechnology Company), aldehyde dehydrogenase (ALDH; 0.5 μg/ml; cat. no. ab131068; Abcam), CD44 (1:1,000; cat. no. ab243894; Abcam), NGF (1 μg/ml; cat. no. ab6199; Abcam), proNGF (1:500; cat. no. ab221609; Abcam), furin (1:1,000; cat. no. 18413-1-AP; Proteintech Group, Inc.) and GAPDH (1:10,000; cat. no. 60004-1-Ig; Proteintech Group, Inc.). Subsequently, incubation with HRP-conjugated secondary antibodies for 1 h at room temperature was performed. The secondary antibodies used were anti-mouse HRP-conjugated IgG (1:4,500; cat. no. AS003; ABclonal Biotech Co., Ltd.) and anti-rabbit HRP-conjugated IgG (1:4,500; cat. no. AS014; ABclonal Biotech Co., Ltd.). Detection was performed using an ECL system (PerkinElmer, Inc.). The target protein levels were normalized to those of GAPDH. The band densities were analyzed using ImageJ software (version 1.50i; National Institutes of Health).

Clinical specimen collection. BC and adjacent (>2 cm from the cancer tissue) non-cancerous breast tissue specimens from 67 female patients (median age, 45 years; range, 32-65 years) enrolled between January 2023 and June 2024 in Shandong Cancer Hospital and Institute, Shandong First Medical University and Shandong Academy of Medical Sciences (Jinan, China) were used in immunoblotting and immunohistochemistry (IHC) experiments. The study protocol was approved by the Institutional Review Board of Shandong Cancer Hospital and Institute, Shandong First Medical University and Shandong Academy of Medical Sciences (approval no. SDTHEC2022009017; Jinan, China). The patient inclusion

criteria were as follows: i) First diagnosis of breast cancer; ii) patients had not received any chemotherapy or hormone treatment; iii) without breast surgery history; and iv) without motion artifact. Breast cancer diagnosis was validated using ultrasound and MRI.

IHC. After being fixed in 10% neutral buffered formalin at room temperature for 24 h, the tissue was embedded in paraffin and cut into 5-μm sections. Tissue sections were dewaxed by treatment with xylene, followed by rehydration in an ethanol gradient (5 min each). Subsequently, the sections were treated with an antigen retrieval solution in a microwave oven for 10 min, incubated in 3% H_2O_2 at 37˚C for 15 min, washed with PBS and blocked with 3% BSA (cat. no. A8020; Beijing Solarbio Science & Technology Co., Ltd.) at room temperature for 30 min. The sections were then incubated with anti-CENPU (1:100; cat. no. 13186-1-AP; Proteintech Group, Inc.), anti-proNGF (1:200; cat. no. ANT-005; Alomone Labs), anti-NGF (1:300; cat. no. ab216419; Abcam) and anti-furin (10 μg/ml; cat. no. ab231573; Abcam) antibodies overnight at 4˚C. Next, the sections were incubated with secondary antibodies (1:1,000; cat. no. ab6721; Abcam) at room temperature for 1 h. The signal was developed using a 3,3'-diaminobenzidine color reagent, and the sections were stained with hematoxylin at 37˚C for 3 min, sealed and observed under a light microscope (Nikon Corporation). Stained slides scanned by Panoramic SCAN II (3DHISTECH, Ltd.) and images were captured by CaseViewer software (version 2.9.0; 3dhistech.com/news/caseviewer-becomes-slideviewer/). The H-score is determined by the formula H-SCORE=∑(PI x I), where PI represents the percentage of cells with a specific staining intensity and I represents the corresponding staining intensity level. Specifically, it is computed as (percentage of weakly-stained cells x1) + (percentage of moderately-stained cells x2) + (percentage of strongly-stained cells x3). The resulting H-score ranges from 0 to 300. The staining intensity and extent of positivity were evaluated using the aforementioned scoring system to provide a semi-quantitative estimation of overall staining patterns. The composite scores were used to compare expression trends among groups.

Transfection. A short hairpin RNA (sh/shRNA) against *CENPU* (sh*CENPU*) and a scrambled control shRNA (CON313) from Syngentech Co., Ltd. were used. The target sequences of the shRNAs were as follows: CON313, 5'-TTC TCCGAACGTGTCACGT-3'; and sh*CENPU*, 5'-CAGGTA TGAGCTATAATAA-3'. Cal51 and MDA-MB-231 cells were infected with shRNA-encoding lentiviruses to generate stable cell lines. The lentiviral transfer vector pLKO.1-puro was utilized within a third-generation system comprising packaging plasmids pMD2.G and psPAX2. Transient transfection was performed in 293T cells (American Type Culture Collection) using Lipofectamine 3000 (Invitrogen; Thermo Fisher Scientific, Inc.) with 4 μg total DNA at a 4:3:1 ratio (transfer vector:psPAX2:pMD2.G). Transfected cells were maintained at 37˚C for 72 h, and viral supernatants were collected at 48/72 h, filtered (0.45 μm) and concentrated by centrifugation (16 h at 6,800 rpm) at 4˚C. Target cells (MDA-MB-231/Cal51) were infected at MOI=10 with 8 μg/ml polybrene for 24 h. Post-transduction, cells underwent puromycin selection (2 μg/ml for MDA-MB-231; 1 μg/ml for Cal51) for 7 days, followed by maintenance at half-selection dose. Functional assays were conducted ≥14 days post-selection to ensure stable expression.

A *CENPU* overexpression plasmid and control plasmid (CON220) from Syngentech Co., Ltd. were also used. Transient transfection of MDA-MB-231 and Cal51 cells used pcDNA3.1(+) with 2 μg plasmid DNA (A260/A280=1.85±0.05) per 35-mm well dish. Transfections employed Lipofectamine 3000 at a 1:2 DNA (μg):reagent (μl) ratio. Cells were incubated with DNA-lipid complexes at 37˚C for 6 h before medium replacement. Further analyses were performed 24-48 h post-transfection.

ELISA. ELISA was performed using MDA-MB-231, Cal51 and T47D cell lysates. Cells were resuspended in PBS at a density of $1x10^6$ cells/ml and subjected to ultrasonication on ice using a Covaris E220 system (Covaris, LLC) under the following parameters: 20 kHz frequency, 10-sec pulses per cycle (3 cycles in total), with 10-sec intervals between pulses. After centrifugation at 2,000-3,000 rpm at 2-8˚C for 20 min, the supernatant was collected and ELISA was performed using an NGF ELISA kit (cat. no. LP-H017695; Shanghai Lanpai Biotechnology Co., Ltd.).

Cell migration and invasion assays. A wound healing assay was performed to assess the migratory potential of cells. MDA-MB-231, Cal51 and T47D cells were seeded in 6-well plates and cultured until the confluency was >90%. After serum starvation, the cells were scratched with a 10-μl pipette tip to artificially create wounds on the cell surface, and were imaged under a light microscope at 0 and 48 h. ImageJ software (version 1.50i) was used for quantification of the wound.

A Matrigel-precoated Transwell chamber (with 8-μm pores) was used for the invasion assay, while the migration assay was performed using Transwell inserts without Matrigel precoating, as previously described (15). A total of 150 μl Matrigel diluent (Matrigel:DMEM=1:8; cat. no. 356234; Corning, Inc.) was spread evenly on the cell inserts, which were placed in a 37˚C and 5% CO_2 incubator until the Matrigel solidified. A total of $5x10^4$ cells/ml were diluted in DMEM without FBS. A total of 150 μl of the diluted cells were placed in the upper layer of the Transwell chamber and 600 μl of DMEM supplemented with 20% FBS was added to the lower chamber. Following incubation (10-12 h for MDA-MB-231 and Cal51 cells and 24-36 h for T47D cells), the cells in the upper chamber were gently wiped with a cotton swab, fixed with 4% paraformaldehyde at room temperature for 15 min, stained with 0.1% crystal violet at room temperature for 15 min and photographed under a light microscope. ImageJ software (version 1.50i) was used for quantification.

Mammosphere formation assay. MDA-MB-231, Cal51 and T47D cells in the logarithmic growth phase were collected, washed twice with serum-free DMEM/F12, counted, and resuspended in DMEM/F12 without serum, supplemented with B27, 20 ng/ml epidermal growth factor and 20 ng/ml basic fibroblast growth factor (all from Invitrogen; Thermo Fisher Scientific, Inc.). A total of $2x10^3$ cells/well were seeded in an ultra-low adhesion culture plate (Corning, Inc.). After

7 days of culture at 37˚C, images were acquired under an inverted light microscope and the mammospheres formed (defined as cell clusters with a diameter ≥30 μm, with clear boundaries and intact morphology) were counted. ImageJ software (version 1.50i) was used for quantification.

Co-immunoprecipitation. Lysates from MDA-MB-231 and Cal51 cells prepared in RIPA buffer (Thermo Fisher Scientific, Inc.) were centrifuged at 12,000 x g, 4˚C for 10 min to remove the debris. Per reaction, 500 μg total protein was incubated overnight with: Anti-CENPU (1:2,000, cat. no. YN1585; ImmunoWay Biotechnology Company), anti-furin (1:1,000, cat. no. ab3467; Abcam), anti-proNGF (1:1,000; cat. no. ab52918; Abcam) or rabbit IgG control (2 μg/reaction; cat. no. 2729; Cell Signaling Technology, Inc.). Immune complexes were captured using the Pierce Co-IP kit (cat. no. 88804; Thermo Fisher Scientific, Inc.) according to the manufacturer's instructions, employing Protein A/G magnetic beads (cat. no. 88802; Thermo Fisher Scientific, Inc.). The precipitated proteins were analyzed by western blotting.

4D-data-independent acquisition (DIA) quantitative proteomics. MDA-MB-231 cell lines transfected with the control vector CON313, with knockdown of the CENPU gene (sh*CENPU*), and overexpression of CENPU were used, and the protein precipitates obtained after acetone precipitation of the cell lysates were collected as experimental samples. The samples were treated with liquid nitrogen and grinded into powder, and were subsequently incubated in lysis buffer (7 M urea, 2 M thiourea, 4% SDS, 40 mM Tris-HCl; pH 8.5) containing 1 mM PMSF and 2 mM EDTA (final concentration) at 4˚C for 5 min. The samples were mixed thoroughly and sonicated using an ultrasonic disruptor at 25% power for 10 min. Subsequently, they were centrifuged at 12,000 x g at 4˚C for 10 min, and the supernatant was collected. Four times the volume of cold acetone was added to the supernatant, and it was allowed to precipitate overnight at -20˚C, followed by centrifugation at 12,000 x g at 4˚C for 5 min. The precipitate was retained, washed with cold acetone, and centrifuged again at 12,000 x g at 4˚C for 5 min. The precipitate was again retained, and the washing step was repeated three times. The protein pellets were air-dried and resuspended in 8 M urea/100 mM triethylammonium bicarbonate (pH 8.0). The BCA protein quantitation assay was used to measure the total protein concentration. Subsequently, protein hydrolysis and desalination are carried out. Liquid chromatography (LC) was performed on a nanoElute UHPLC (Bruker Corporation). In total, ~200 ng peptides were separated within 40 min at a flow rate of 0.3 μl/min on a commercially available reverse-phase C18 column with an integrated CaptiveSpray Emitter (25 cm x 75 μm; 1.6 μm particle size; Aurora Series with CSI; IonOpticks). The separation temperature was kept by an integrated Toaster column oven at 50˚C. Mobile phases A and B were produced with 0.1% formic acid in water and 0.1% formic acid in acetonitrile. Mobile phase B was increased from 2 to 22% over the first 25 min, increased to 35% over the next 5 min, further increased to 80% over the next 5 min, and then held at 80% for 5 min. The LC process was coupled online to a hybrid timsTOF Pro2 mass spectrometer via a CaptiveSpray nano-electrospray ion source (Bruker Corporation). To establish the applicable acquisition windows, timsTOF Pro2 was operated in Data-Independent Parallel Accumulation-Serial Fragmentation (PASEF) mode with four PASEF MS/MS frames in one complete frame. The capillary voltage was set to 1,500 V, and the MS and MS/MS spectra were acquired from 100 to 1,700 m/z. As for ion mobility range (1/), 0.85 to 1.3 Vs/was used. The 'target value' of 10,000 was applied to a repeated schedule, and the intensity threshold was set at 2,500. The range of charge state was set from 0 to 5. The collision energy was ramped linearly as a function of mobility from 45eV at 1/=1.3 Vs/to 27 eV at 1/=0.85 Vs/. The quadrupole isolation width was set to 2 Thomson for m/z <700 and 3 Th for m/z >800. Raw mass spectrometry data were analyzed with DIA-NN software (v1.8.1) (https://github.com/vdemichev/DiaNN) using the library-free method. The *Homo sapiens* SwissProt database (https://www.uniprot.org/; 20,425 entries) was used to create a spectral library with deep learning algorithms of neural networks. Match Between Runs was applied to align precursor retention times and m/z values across DIA runs, enabling cross-run matching of peptide identifications; a spectral library from DIA data was created and the data were reanalyzed using this library. To comprehensively elucidate the functional characteristics of various proteins, R software (clusterProfiler) version 3.10.1 (https://bioconductor.org/packages/clusterProfiler) was employed to conduct functional annotation and enrichment analysis on both the identified proteins and differentially expressed proteins in each comparison group. This analysis encompassed Kyoto Encyclopedia of Genes and Genomes (KEGG) and Disease Ontology (DO) (Fig. S1A and B), wherein all differentially expressed proteins were mapped to the corresponding terms in the KEGG (https://www.kegg.jp/) and DO (http://www.disease-ontology.org/) databases. The number of proteins associated with each term was calculated, followed by a hypergeometric test (equivalent to Fisher's exact test; implemented in the R stats package version 4.3.2; https://www.r-project.org/) to identify significantly enriched KEGG and DO terms among the differentially expressed proteins. KEGG/DO terms were considered significantly enriched if they met FDR-adjusted $P<0.05$ and fold change >2 (log2FC >1).

Flow cytometry. MDA-MB-231, Cal51 and T47D cells were used for the experiment. After resuspending the cells with PBS, the proportion of $CD24^{-}CD44^{+}$ cells was detected using a flow cytometer. The cells were incubated with CD44 APC (1:40; cat. no. 559942; BD Biosciences) and CD24 PE (1:50; cat. no. 555428; BD Biosciences) at 4˚C for 30 min in the dark. Isotype controls, APC IgG (1:100; cat. no. 555751; BD Biosciences) and PE IgG (1:100; cat. no. 555749; BD Biosciences), were incubated under the same conditions. A BD FACSCanto II flow cytometer (BD Biosciences) was used for data acquisition, and the data were analyzed using FlowJo v10.8.1 (Becton, Dickinson and Company).

Furin activity measurement. Furin activity in MDA-MB-231, Cal51 and T47D cells was measured by assessing the ability of the cells to digest pERTKR-MCA. Briefly, each cell extract

was incubated with pERTKR-MCA (100 M) in a solution composed of 25 mM Tris, 25 mM methyl-ethane-sulfonic acid and 2.5 mM $CaCl_2$ (pH 7.4) at 37˚C. Measurements were taken every 5 min for a total duration of 100 min. At a pH of 6.0 and a Ca2+ concentration of 1 mM, the catalytic activity of furin was dynamically detected using a fluorometer. The K_m value was derived from the Michaelis-Menten curve fitted to the enzymatic activity data (velocity vs. substrate concentration). In the present study, K_m is indirectly reflected by the substrate concentration at which the reaction velocity reaches half of V_{max}. A spectrofluorometer (FLUOstar OPTIMA; BMG Labtech GmbH) was used for analysis. A furin inhibitor, decanoyl-RVKR-chloromethyl ketone (DECRVKR-CMK) purchased from Calbiochem (Merck KGaA), was used at a concentration of 10 μM. Cells were treated with this inhibitor at 37˚C for 7 days.

Reverse transcription-quantitative PCR. Total RNA from cells in each group was extracted using the TRIzol® reagent (Invitrogen; Thermo Fisher Scientific, Inc.). First-strand cDNA synthesis was carried out according to the manufacturer's instructions with a first-strand cDNA synthesis kit (Applied Biosystems; Thermo Fisher Scientific, Inc.). Primer Express software (version 3.0; Applied Biosystems; Thermo Fisher Scientific, Inc.) was utilized to design gene-specific primers for each target gene. The primer sequences were as follows: CENPU: 5'-GAAAAGAAAAGGCAGCGTA TGA-3' (forward) and 5'-AATATGCTGCATTCCTAAG GGA-3' (reverse); GAPDH: 5'-GGAGCGAGATCCCTCCAA AAT-3' (forward) and 5'-GGCTGTTGTCATACTTCTCA TGG-3' (reverse). The reaction conditions included pre-denaturation at 95˚C for 2 min, denaturation at 95˚C for 30 sec, annealing at 60˚C for 30 sec, and extension at 72˚C for 30 sec for a total of 40 cycles. CENPU mRNA expression was calculated using the $2^{-\Delta\Delta Cq}$ method (26).

Xenograft model. The experimental protocol was approved by the Animal Care Committee of Shandong Cancer Hospital and Institute, Shandong First Medical University and Shandong Academy of Medical Sciences (approval no. SDTHEC2022009018; Jinan, China). To investigate the tumorigenic potential of Cal51-sh*CENPU* and Cal51-CON313 cells at varying concentrations, $1x10^6$, $1x10^5$, $1x10^4$ and $1x10^3$ cells (resuspended in PBS) were injected into the mammary fat pads of NSG mice (27,28). NSG mice were obtained from Nanjing Biomedical Research Institute of Nanjing University. A total of 32 mice (4-6 weeks old; female; 18-20 g) were randomly divided into 8 groups (n=4/group). Mice were maintained under specific-pathogen-free (SPF) conditions (temperature, 25±1˚C; humidity, 55±5%; 12/12-h light/dark cycle) with *ad libitum* access to irradiated food and autoclaved water. The tumor sizes formed by the Cal51-sh*CENPU* and Cal51-CON313 cell groups at these different concentrations were measured and subjected to statistical analysis to determine significant differences. MDA-MB-231-sh*CENPU* and MDA-MB-231-CON313 cells ($1x10^6$ cells/specimen; resuspended in PBS) were injected into the fat pads of 4-week-old female nude mice (Nanjing Biomedical Research Institute of Nanjing University). A total of 15 female nude mice (age, 4 weeks; weight, 16-18 g) were randomly divided into 3 groups (n=5/group). Mice were maintained under SPF conditions (temperature: 25±2˚C; humidity: 50±10%; 12/12-h light/dark cycle) with free access to autoclaved food and acidified water. The tumor dimensions were measured at 3-day intervals for 21 days. When the size of each tumor was ~100 mm^3, MDA-MB-231-CON313 mice were intraperitoneally injected with a furin inhibitor (5 mg/kg DECRVKR-CMK) three times per week for 3 weeks. The following humane endpoints were predefined in the present study: i) Clear signs of pain or unremitting suffering; ii) rapid weight loss; iii) persistent lack of appetite or abnormal behavior; and iv) inability to stand or extreme weakness after excluding anesthesia-related reasons (however, no anesthesia was administered to the mice in the present study). However, during the experiment no such signs were observed, indicating that the tumors did not severely affect the health of the mice until the end of the study. The tumor volumes were calculated using the following formula: Volume=0.5 x (width^2 x length). The maximum tumor volume observed in the first experiment (Cal51 cells) was 936 mm^3, and the maximum diameter was 1.3 cm. The maximum tumor volume observed in the second experiment (MDA-MB-231 cells) was 1,764 mm^3, and the maximum diameter was 1.8 cm. At study completion, the mice were euthanized using CO_2 inhalation in accordance with the American Veterinary Medical Association 2020 Guidelines (29). The procedure involved an initial concentration of 30% CO_2, a flow rate controlled at 50% of the chamber volume per minute, and a gradual increase to 70% to ensure rapid and humane loss of consciousness. Death was confirmed by observing pupillary dilation and cessation of cardiac activity. The tumors were then extracted, measured and used for subsequent evaluation.

Statistical analysis. Statistical processing was implemented with SPSS software v18.0 (SPSS, Inc.). Intergroup comparisons were performed using unpaired Student's t-test (two-group comparisons) or one-way ANOVA (multi-group comparisons) followed by the Least Significant Difference pos hoc test (for equal variances between groups). When two types of treatment were used, a two-way ANOVA followed by Sidak post hoc test was performed. All statistical differences were established using two-tailed probability measures. Experimental procedures were replicated in triplicate, and the data are presented as the mean ± SD. $P<0.05$ was considered to indicate a statistically significant difference.

Results

CENPU is expressed at high levels in breast invasive ductal carcinoma. Our previous study showed that CENPU was markedly upregulated in TNBC tissues compared with luminal breast cancer tissues, and this upregulation was associated with a poor prognosis (15). The present study examined whether CENPU expression is associated with the degree of invasiveness in BC. A total of 67 tissue samples were collected, including 17 cases of breast dysplasia, 20 cases of ductal carcinoma *in situ* and 30 cases of invasive ductal carcinoma. IHC results confirmed that CENPU expression was positively associated with the degree of invasiveness in BC (Fig. 1A and C). Next, four normal breast tissue samples

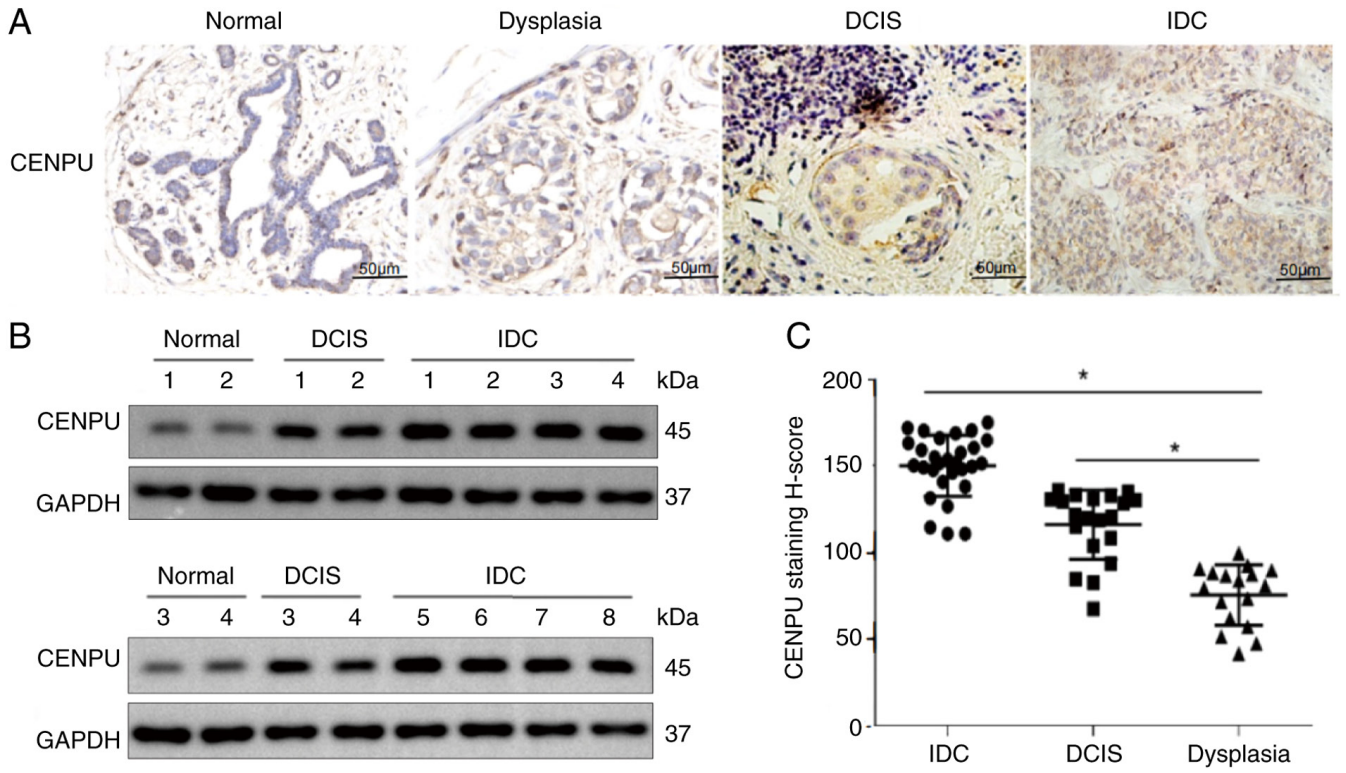

Figure 1. Expression levels of CENPU are positively associated with the degree of invasiveness in breast cancer. (A) Immunohistochemical staining and. (B) Western blotting was performed using four samples of normal breast tissue, four samples of DCIS tissue and eight samples of IDC tissue. (C) Quantification of tissue collected from 67 patients (17 patients with breast dysplasia, 20 patients with DCIS and 30 patients with IDC) was performed. Scale bar, 50 μm. *P<0.05. CENPU, centromere protein U; IDC, invasive ductal carcinoma; DCIS, ductal carcinoma *in situ*.

(adjacent tissues of the same patients with BC), four ductal carcinoma *in situ* tissue samples and eight breast invasive ductal carcinoma tissue samples were used to verify the findings by western blotting. The results demonstrated that compared with the normal breast and ductal carcinoma *in situ* tissue samples, the invasive ductal carcinoma tissues exhibited higher CENPU levels (Fig. 1B).

CENPU promotes the stem cell-like properties of BCSCs. Cancer stem cells serve an important role in tumorigenesis and recurrence. Given that our previous study showed that high CENPU expression was associated with poor overall survival (15), it was assessed whether CENPU expression promotes the stem cell-like properties of BCSCs. Firstly, the overexpression efficiency of CENPU in cells was verified through PCR or western blotting (Fig. S2). Subsequently, a $CD24^-$ $CD44^+$ cell identification experiment and a mammosphere formation assay were performed to determine the association between CENPU expression and the stem cell-like properties of BCSCs. Western blotting revealed that CD44 and ALDH (30,31) were downregulated in *CENPU*-knockdown MDA-MB-231 and Cal51 cells, where it had been confirmed that CENPU was highly expressed in our previous study (15) (Fig. 2A and B), and upregulated in *CENPU*-overexpressing T47D cells, where it had been confirmed that CENPU was expressed at a low level (15) (Fig. 2C).

The mammosphere generation assay showed that *CENPU* knockdown decreased the number and volume of mammospheres (Fig. 2E). Conversely, *CENPU* overexpression markedly enhanced the number and volume of mammospheres (Fig. 2G). *CENPU* knockdown reduced the rate of $CD24^-$ $CD44^+$ cells (30,32,33) (Fig. 2D and F), whereas *CENPU* overexpression exerted a contrasting effect (Fig. 2H). The aforementioned data indicated that *CENPU* overexpression promoted the stem cell-like properties of BCSCs.

The role of CENPU in BC progression was examined using wound healing and Transwell assays, to determine the effect of CENPU on cell migration and invasion. *CENPU* knockdown inhibited the migratory and invasive potential of MDA-MB-231 and Cal51 cells (Fig. 2I, J, L and M), whereas *CENPU* overexpression enhanced the migratory and invasive potential of T47D cells (Fig. 2K and N).

CENPU promotes the maturation conversion of proNGF to NGF. Comparative DO and KEGG enrichment analyses of MDA-MB-231 cell lines with CENPU knockdown (sh*CENPU*) and overexpression revealed that CENPU is significantly associated with BC and related cancer signaling pathways. (Fig. S1A and B), while 4D-DIA quantitative differential protein enrichment analysis showed that the sh*CENPU* group exhibited notably lower NGF expression compared with the CON313 group (Fig. S1C). NGF is a critical neurotrophic factor that controls differentiation and survival in target neurons. NGF matures upon undergoing furin-mediated protease cleavage of its proNGF form (34). Therefore, western blotting and an ELISA were performed to examine whether CENPU knockdown and overexpression affect the expression of NGF and proNGF. Western blotting and ELISA results revealed that

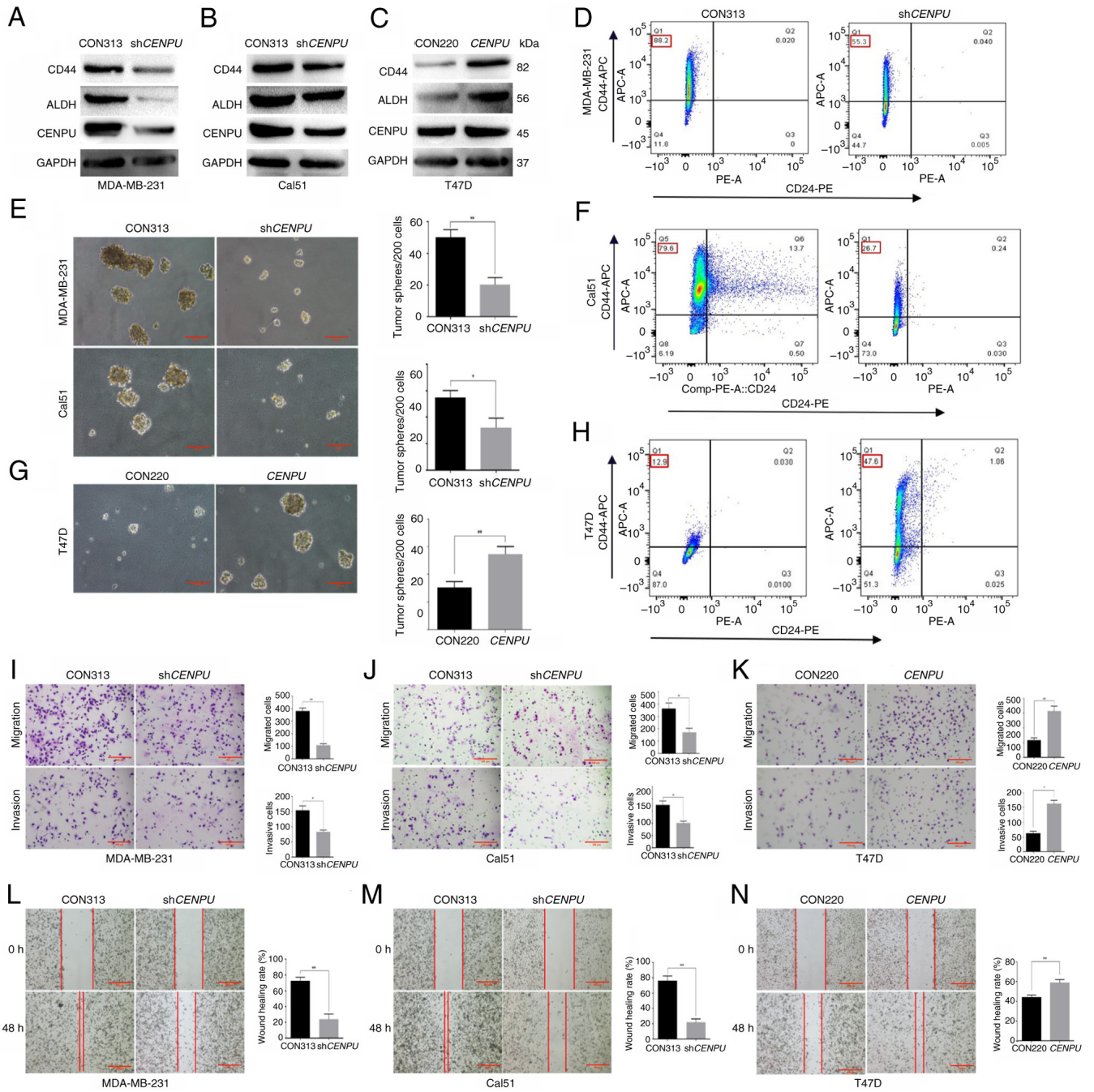

Figure 2. CENPU promotes tumorigenesis, stem cell-like properties, migration and invasion in breast cancer cells. Western blotting was performed to detect the expression levels of CD44 and ALDH in (A) MDA-MB-231, (B) Cal51 and (C) T47D cells with different CENPU expression levels. Association between CENPU expression and the number of mammospheres per 200 cells in (E) MDA-MB-231 and Cal51 cells and (G) T47D cells (scale bar, 100 μm). $CD24^-CD44^+$ flow cytometry results showed that CENPU expression levels affected the percentage of the $CD24^-CD44^+$ population among (D) MDA-MB-231, (F) Cal51 and (H) T47D cells. Transwell assays were performed to determine the effect of CENPU levels on the migration and invasiveness of (I) MDA-MB-231, (J) Cal51 and (K) T47D cells (scale bar, 200 μm). A wound healing assay was performed to determine the effect of CENPU on the migration potential of (L) MDA-MB-231, (M) Cal51 and (N) T47D cells (scale bar, 200 μm). *P<0.05; **P<0.01. CENPU, centromere protein U; sh, short hairpin RNA; APC, allophycocyanin; ALDH, aldehyde dehydrogenase; PE, phycoerythrin.

NGF expression was markedly suppressed in MDA-MB-231 and Cal51 cells with *CENPU* knockdown (Fig. 3A, B, D and E). Conversely, NGF expression was markedly enhanced upon *CENPU* upregulation in *CENPU*-overexpressing T47D cells (Fig. 3C and F). Furthermore, the changes in CENPU expression affected proNGF and NGF expression in contrasting manners. MDA-MB-231-sh*CENPU*, Cal51-sh*CENPU* and T47D-*CENPU* cells, and their corresponding controls, were treated with NGF-neutralizing antibodies. The ability of CENPU to promote migration, invasion and mammosphere formation was significantly suppressed when the cells were treated with NGF-neutralizing antibodies (Fig. 3G-L). No significant differences were observed between each overexpression or knockdown group and the corresponding control treated with NGF. This indicated that NGF may serve a critical role in the CENPU-induced promotion of BC induction and progression.

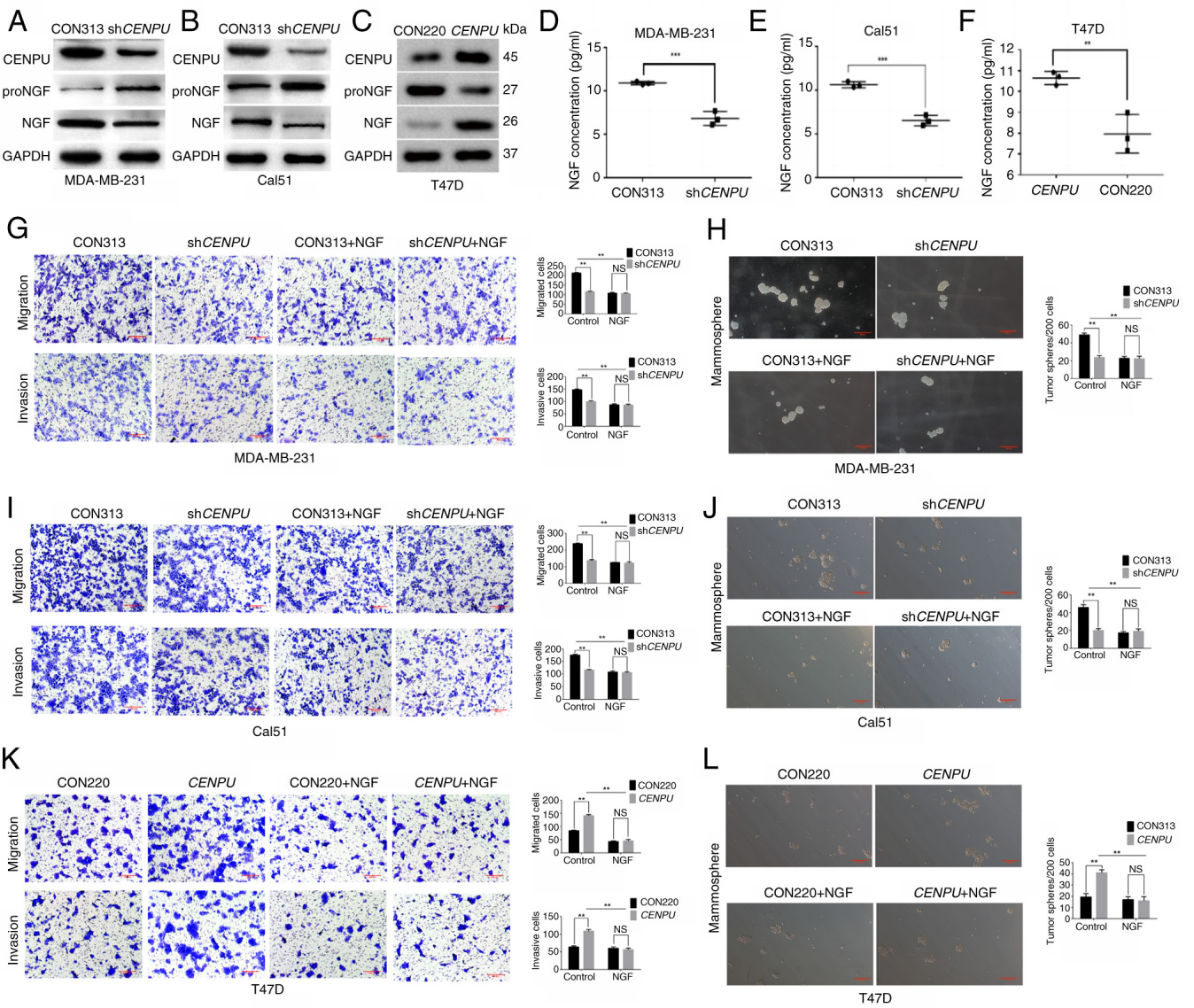

Figure 3. CENPU promotes the conversion of proNGF to NGF. Western blotting experiments were performed to detect the expression of NGF and proNGF in (A) MDA-MB-231-sh*CENPU*, (B) Cal51-sh*CENPU* and (C) T47D-*CENPU* cells and their corresponding control groups. The intracellular NGF levels in (D) MDA-MB-231, (E) Cal51 and (F) T47D cells after 48 h of treatment were analyzed by ELISA using ultrasonicated cell supernatants. After NGF-neutralizing antibodies were added to (G) MDA-MB-231-sh*CENPU*, (I) Cal51-sh*CENPU* and (K) T47D-*CENPU* cells, and their corresponding control groups, Transwell migration and invasion assays were conducted (scale bar, 200 μm). After NGF-neutralizing antibodies were added to the (H) MDA-MB-231-sh*CENPU*, (J) Cal51-sh*CENPU* and (L) T47D-*CENPU* cells, and their corresponding control groups, a mammosphere formation assay was performed to measure the number of mammospheres per 200 cells that formed (scale bar, 100 μm). *P<0.05; **P<0.01. CENPU, centromere protein U; sh, short hairpin RNA; NGF, nerve growth factor; proNGF, NGF precursor; NS, not significant.

CENPU promotes NGF maturation by enhancing the enzymatic activity of furin. The previous experiment demonstrated that CENPU could affect the expression levels of proNGF and NGF. Furin is the sole enzyme capable of cleaving proNGF, thereby facilitating its conversion into NGF. Therefore, it was examined whether CENPU regulates the expression of proNGF and NGF by affecting furin activity. Western blotting revealed lower furin expression levels in sh*CENPU*-expressing MDA-MB-231 and Cal51 cells, and higher furin expression levels in *CENPU*-overexpressing T47D cells (Fig. 4A). Next, furin activity was assayed by measuring the fluorescence intensity of the furin-specific fluorescence substrate pERTKR-MCA. Furin activity was suppressed in sh*CENPU*-expressing MDA-MB-231 and Cal51 cells, and elevated in *CENPU*-overexpressing T47D cells (Fig. 4B).

There are two methods to increase enzymatic activity: i) Increasing the enzyme concentration; and ii) increasing the affinity of the enzyme to the substrate, as indicated by the Michaelis constant (K_m). The K_m value is known as the meter constant, which refers to the substrate concentration of the reaction that reaches $1/2V_{max}$, where V_{max} is the reaction velocity. K_m is generally expressed in mol/l, and this index is only determined by the intrinsic characteristics of the enzyme but is independent of its concentration. The larger the K_m value, the smaller the affinity of the enzyme to the substrate. Using the double reciprocal plotting method, 1/V is plotted against 1/[S] (where S is the substrate concentration) to generate

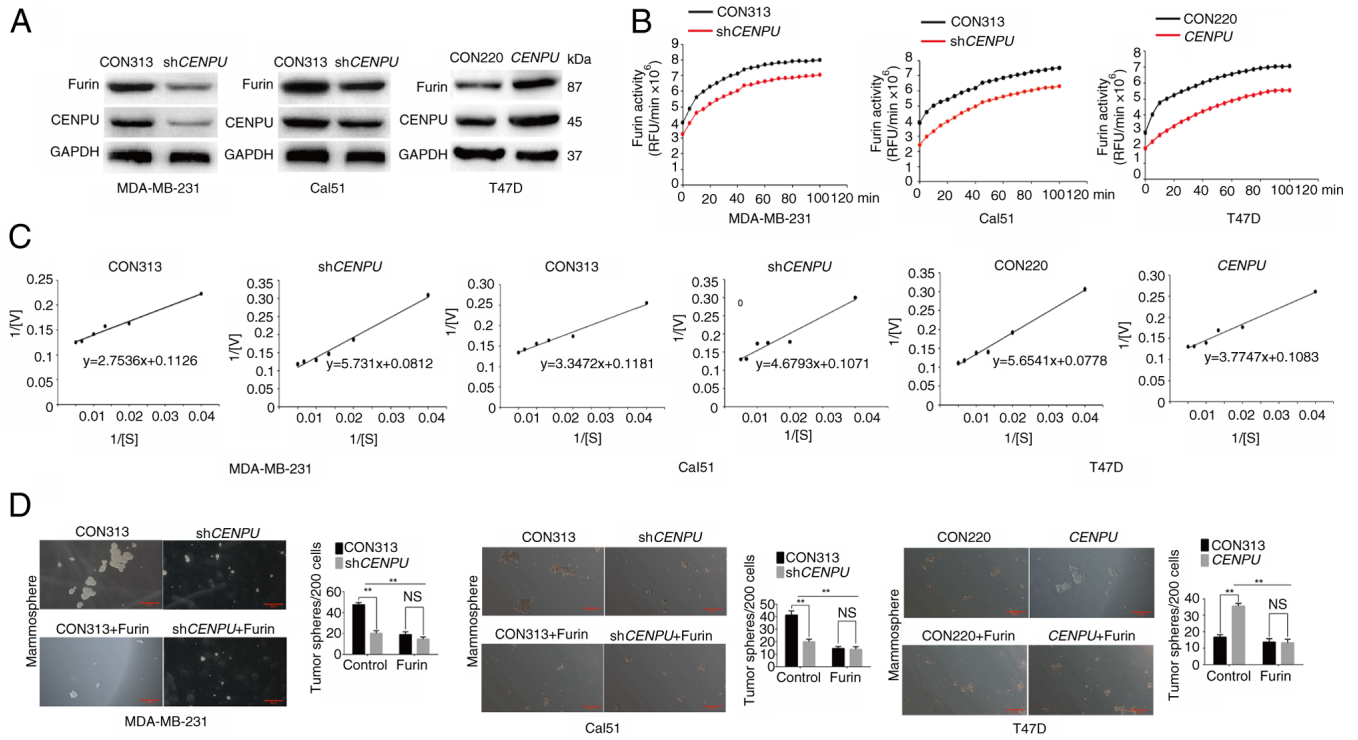

Figure 4. CENPU enhances the activity of furin. (A) Western blotting was performed to determine the expression levels of furin in MDA-MB-231, Cal51 and T47D cells. (B) Furin activity in MDA-MB-231, Cal51 and T47D cells was measured based on fluorescence intensity. (C) Michaelis constant values in the experimental group and control group of MDA-MB-231, Cal51 and T47D cells were obtained using double reciprocal plotting. (D) Mammosphere formation assays were performed after treatment with a furin inhibitor, and the number of tumor spheres per 200 cells was quantified (scale bar, 100 μm). **P<0.01. CENPU, centromere protein U; sh, short hairpin RNA; NS, not significant; RFU, relative fluorescence units; V, reaction velocity; S, substrate concentration.

a straight line. The y-intercept of the line is $1/V_{max}$, and the x-intercept is the absolute value of $1/K_m$ (35). At a pH of 6.0 and Ca^{2+} concentration of 1 mM, the K_m value of pERTKR-MCA for furin in sh*CENPU*-expressing MDA-MB-231 cells was 68.63 μmol/l. The K_m in the control group was 24.45 μmol/l. The K_m values of pERTKR-MCA for furin were 43.70 μmol/l in sh*CENPU*-expressing Cal51 cells and 24.45 μmol/l in the control group. The K_m values of pERTKR-MCA for furin were 34.86 and 72.67 μmol/l in the *CENPU*-overexpressing T47D cells and the control group, respectively (Fig. 4C). These results showed that *CENPU* knockdown could reduce the affinity of furin for its substrates, whereas *CENPU* overexpression could increase this affinity.

MDA-MB-231-sh*CENPU*, Cal51-sh*CENPU* and T47D-*CENPU* cells, and their corresponding controls, were treated with a furin inhibitor. The results of the mammosphere formation experiment indicated that the ability of CENPU to promote mammosphere formation was inhibited when the cells were treated with a furin inhibitor (Fig. 4D). No significant differences were observed between each overexpression or knockdown group and the corresponding control treated with furin.

CENPU enhances furin activity by inhibiting its degradation in the lysosomal pathway. The previous experiment showed that CENPU could influence both furin expression and activity. The presence of two conserved LXXLL sequences and two superhelical zinc finger structures at the C-terminal of CENPU suggest that CENPU may form a dimer with other proteins and act as a receptor-binding protein in signal transduction (36). CENPU and furin co-immunoprecipitated with each other in MD-MB-231 and Cal51 cells (Fig. 5A). Using co-immunoprecipitation, it was also demonstrated that furin formed protein complexes with proNGF (Fig. 5B).

The precise mechanism by which CENPU upregulated furin expression in BC cells was then explored. We hypothesized that CENPU interacts with furin to inhibit its degradation. *CENPU* knockdown promoted furin degradation in MDA-MB-231 and Cal51 cells treated with cycloheximide, a protein biosynthesis inhibitor, at indicated at 4, 8 and 12 h after treatment (Fig. 5C, D, I and J). The proteasomal and lysosomal pathways are key pathways regulating protein degradation in cells (37). Therefore, the potential pathways involved in CENPU-regulated furin degradation were investigated. Proteasome suppression by MG132 did not affect furin degradation in cells with *CENPU* knockdown compared with the control group (Fig. 5E, F, K and L). However, the suppression of lysosomal activity by chloroquine further inhibited furin degradation in MDA-MB-231-sh*CENPU* and Cal51-sh*CENPU* cells (Fig. 5G, H, M and N). The aforementioned findings indicated that CENPU suppressed furin degradation via the lysosomal pathway.

CENPU promotes tumorigenesis in TNBC in vivo. Since an important function of CENPU in tumorigenesis in the cultured cells was identified, the role of CENPU in a mouse xenograft model was then examined. Female NSG mice were injected with Cal51-sh*CENPU* and Cal51-CON313 cells to determine whether CENPU promotes tumorigenesis

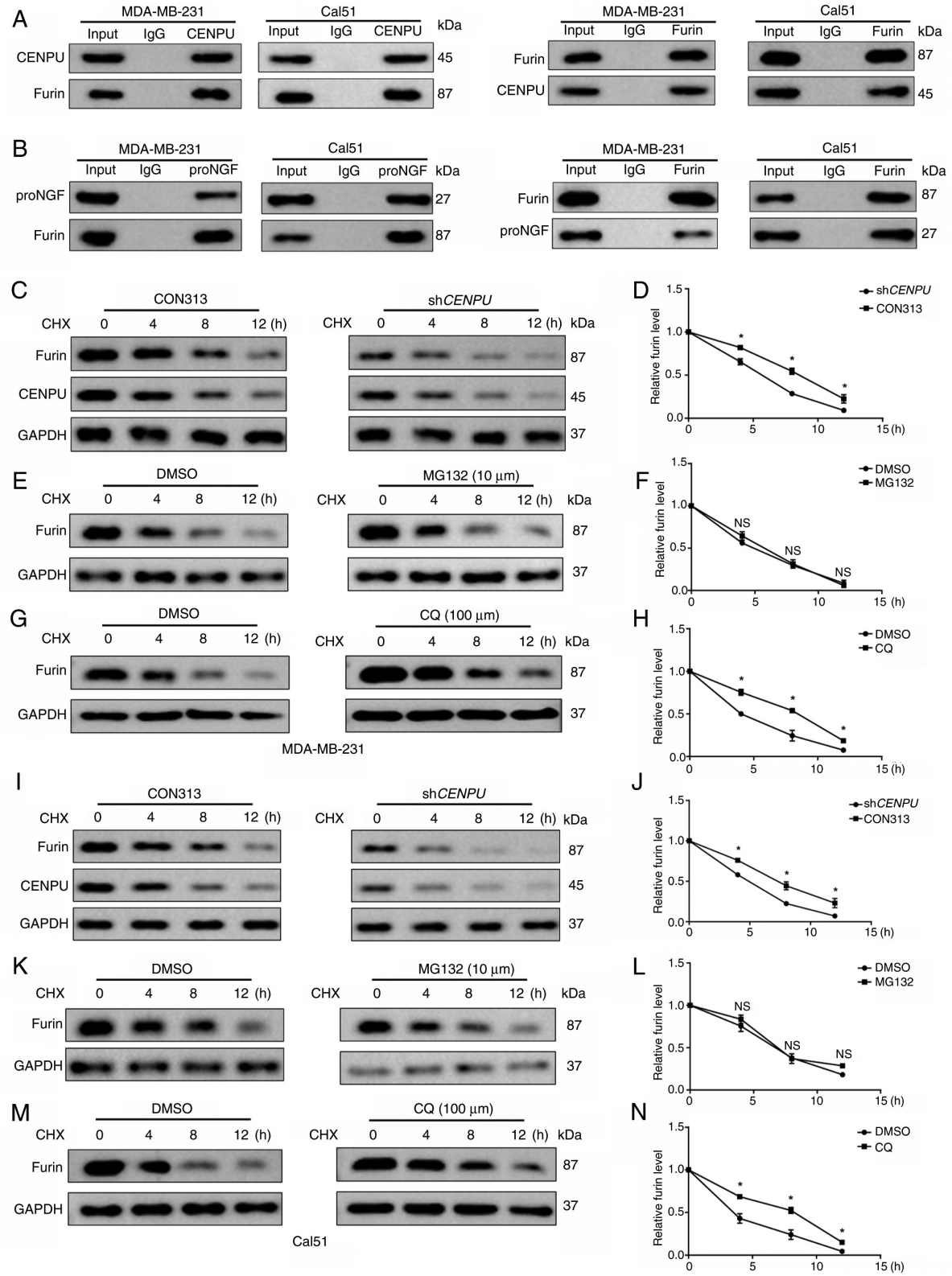

Figure 5. CENPU enhances furin activity by inhibiting its degradation via the lysosomal pathway. (A) CENPU and furin were subjected to co-immunoprecipitation. (B) Furin and proNGF were subjected to co-immunoprecipitation. (C) MDA-MB-231-sh*CENPU* cells and their corresponding controls were treated with CHX (20 μM) for the specified duration, and protein levels were measured by western blotting. (D) Relative expression of furin. (E) MDA-MB-231 cells were treated with MG132 (10 μM) for 12 h, and then also treated with CHX (20 μM) for the indicated times. Protein levels were detected by western blotting. (F) Relative expression of furin. (G) MDA-MB-231 cells were treated with CQ (100 μM) for 12 h, and then treated with CHX (20 μM) for the indicated times. Protein levels were detected by western blotting. (H) Relative expression of furin. (I) Cal51-sh*CENPU* cells and their corresponding controls were treated with CHX (20 μM) for the specified duration, and protein levels were measured by western blotting. (J) Relative expression of furin. (K) Cal51 cells were treated with MG132 (10 μM) for 12 h, and then treated with CHX (20 μM) for the indicated times. Protein levels were detected by western blotting. (L) Relative expression of furin. (M) Cal51 cells were treated with CQ (100 μM) for 12 h, and then treated with CHX (20 μM) for the indicated times. Protein levels were detected by western blotting. (N) Relative expression of furin. *P<0.05 vs. DMSO or CON313 group. The experimental and control groups in panels C-M were run on the same gel/membrane and incubated with the corresponding primary antibodies simultaneously. CENPU, centromere protein U; sh, short hairpin RNA; NS, not significant; proNGF, nerve growth factor precursor; CHX, cycloheximide; CQ, chloroquine.

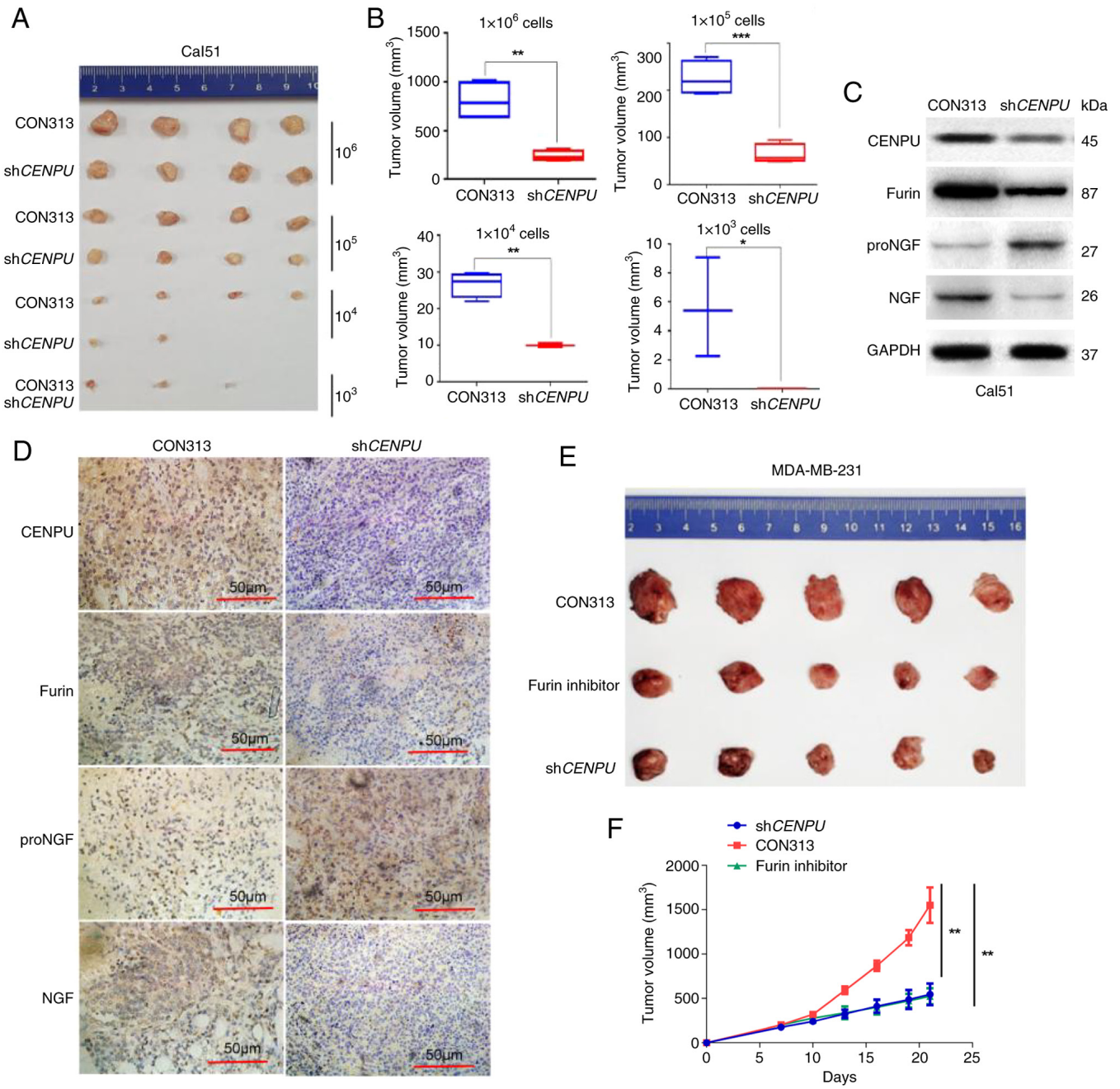

Figure 6. *CENPU* knockdown can inhibit tumorigenesis. (A) A total of 1x10^6, 1x10^5, 1x10^4 and 1x10^3 Cal51-sh*CENPU* and Cal51-CON313 cells were injected into the mammary fat pad of NSG mice. (B) Sizes of the tumors formed in the Cal51-sh*CENPU* and Cal51-CON313 groups using different cell concentrations were measured and statistically analyzed. The tumor tissues collected from the Cal51-sh*CENPU* and Cal51-CON313 groups were (C) analyzed by western blotting and (D) subjected to immunohistochemical staining (scale bar, 50 μm). (E) A total of 1x10^6 MDA-MB-231-sh*CENPU* and MDA-MB-231-CON313 cells were injected into the mammary fat pad of nude mice. When the tumor size was ~100 mm^3, the MDA-MB-231-CON313 mice were administered a furin inhibitor (DECRVKR-CMK) by intraperitoneal injection. (F) The volume of the final tumor was measured, indicating that the furin inhibitor significantly inhibited tumor growth in the MDA-MB-231-CON313 mice. Scale bar, 50 μm. *P<0.05; **P<0.01; ***P<0.001. CENPU, centromere protein U; sh, short hairpin RNA; NS, not significant; NGF, nerve growth factor; proNGF, NGF precursor.

in vivo. The mice injected with 1x10^4, 1x10^5 and 1x10^6 cells with stable *CENPU* knockdown exhibited smaller xenograft tumors compared with that injected with CON313. None of the mice injected with 1x10^3 cells with stable *CENPU* knockdown exhibited formation of xenograft tumors. This suggested that *CENPU* knockdown inhibited tumorigenesis (Fig. 6A and B). IHC and western blotting experiments showed that the furin and NGF protein levels were considerably lower, and the proNGF protein level was higher in sh*CENPU*-Cal51 tumor samples compared with the control samples (Fig. 6C and D).

Furin inhibitor treatment can inhibit CENPU-induced tumor growth. MDA-MB-231-sh*CENPU* and MDA-MB-231-CON313 cells were injected into the mammary fat pads of nude mice. When the tumor size was ~100 mm^3, MDA-MB-231-CON313 mice were intraperitoneally injected with the furin inhibitor DECRVKR-CMK. The furin inhibitor could

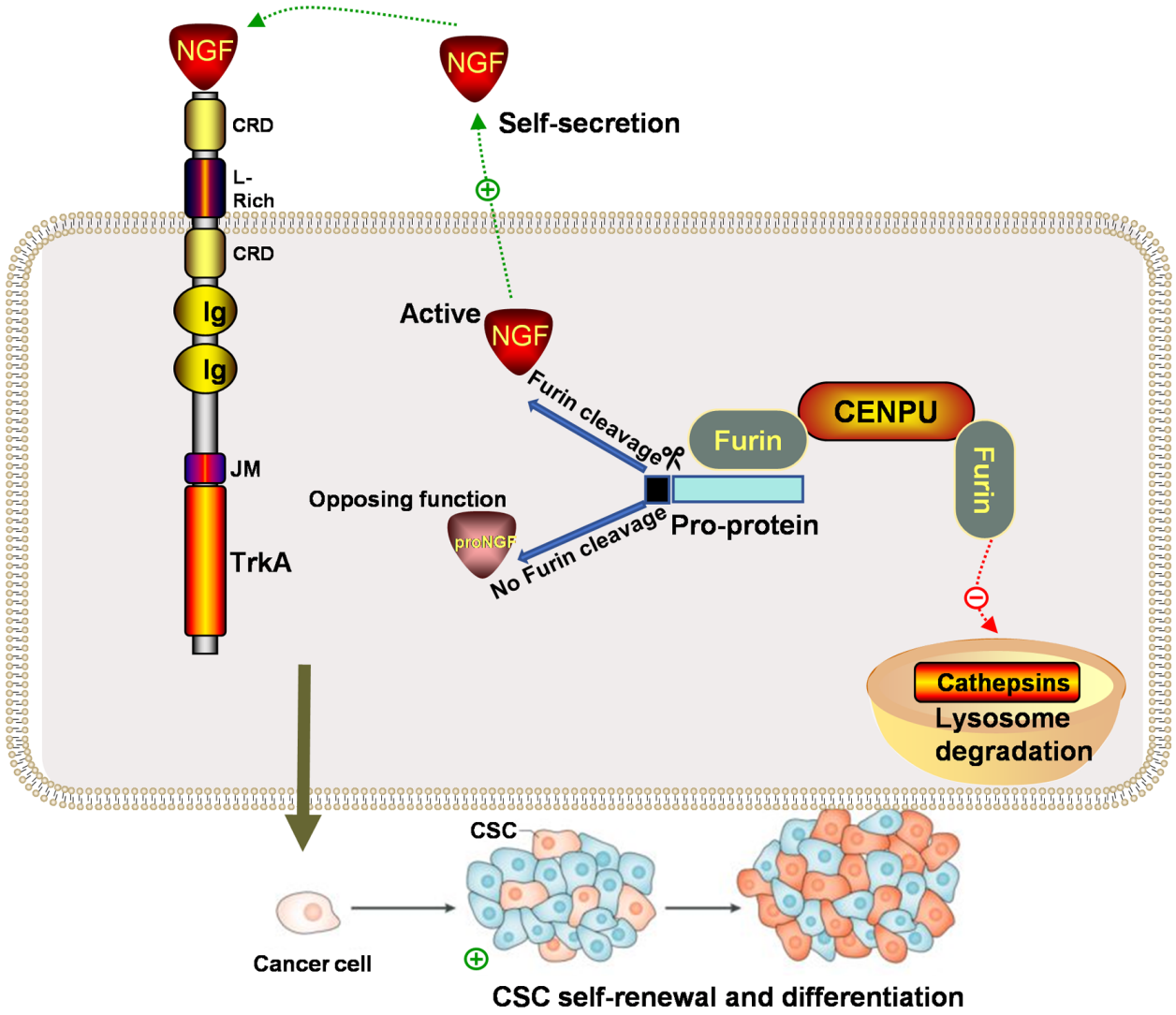

Figure 7. Illustration of the proposed mechanism by which CENPU promotes triple-negative breast cancer invasion, tumorigenesis and breast CSC properties through the furin-proNGF-NGF signaling pathway. CENPU, centromere protein U; NGF, nerve growth factor; proNGF, NGF precursor; CSC, cancer stem cell; TrKA, tropomyosin receptor kinase A; CRD, cysteine-rich domain; JM, juxtamembrane domain.

significantly inhibit CENPU-induced tumor growth. This observation corroborated the aforementioned *in vitro* findings (Fig. 6E and F).

Discussion

The present study identified a potential role of CENPU in TNBC tumorigenesis. Furthermore, the molecular mechanism by which CENPU potentially promotes TNBC tumorigenesis and the stem cell-like properties of BCSCs by enhancing NGF maturation was also established. Specifically, the current study showed that CENPU inhibited the lysosomal degradation of furin, and could bind to the furin protein, increase its expression and enhance its enzymatic activity. The enhancement of furin activity promoted the maturation and transformation of proNGF into NGF. NGF promoted the BCSC-like properties of TNBC cells (Fig. 7). Collectively, these data provided novel insights into how CENPU may promote TNBC tumorigenesis and the stem cell-like properties of TNBC cells.

Our previous study reported that CENPU was notably upregulated in BC tissues compared with adjacent normal breast tissues and expressed at higher levels in TNBC than in luminal BC (15). The present showed that CENPU expression was significantly associated with the degree of invasiveness in BC. The effects of CENPU on TNBC tumorigenesis, BCSC properties, migration and invasion were further investigated, and the results demonstrated that CENPU promoted these features.

CD44 is a multifunctional class I transmembrane glycoprotein. In BCSCs, its expression is linked to self-renewal, tumorigenesis, adhesion, invasion and metastasis. The $CD44^{+}CD24^{-}$-low phenotype is widely used as a marker for BCSC identification and isolation. ALDH1A1, as a stem cell marker, has a high expression level in BCSCs and can promote proliferation and spheroid formation (30-32). The present study demonstrated that knockdown of CENPU reduced the proportion of $CD44^{+}CD24^{-}$ cells, while western blotting analysis revealed downregulation of CD44 and ALDH expression. Conversely, overexpression of CENPU

exhibited the opposite effect. Therefore, we hypothesize that overexpression of CENPU can promote the stem-like characteristics of BCSCs.

NGF is a critical neurotrophic factor that regulates the differentiation and survival of target neurons (25). NGF is biosynthesized as proNGF, and NGF maturation involves furin-associated protease cleavage (38). Hayakawa *et al* (39) reported that NGF promoted gastric cancer development by altering cholinergic signaling. Tomellini *et al* (40) demonstrated that NGF promoted symmetric self-renewal, quiescence and epithelial-to-mesenchymal transition, thereby enlarging the BCSC compartment. In the present study, NGF expression decreased with a decrease in the CENPU level, whereas proNGF expression increased. Furthermore, after NGF-neutralizing antibodies were added to the culture medium of BC cells, the ability of CENPU to promote BC migration, invasion and mammosphere formation was inhibited. Therefore, we hypothesize that CENPU may promote NGF maturation.

Furin is a precursor protein-processing enzyme that helps process multiple bioactive polypeptides or protein precursors in the brain, glands and other peripheral tissues (41). There are large volumes of furin present in tumor tissues, and studies have shown that furin expression increases with the tumor proliferation rate (24,42,43). Furthermore, furin inhibition suppresses the proliferation and infiltration of tumor cells (44-46). The present results showed that CENPU inhibited the lysosomal degradation of furin, bound to furin and increased its expression, thereby enhancing its enzymatic effect on proNGF. A furin inhibitor (DECRVKR-CMK), which was administered in both *in vivo* and *in vitro* settings, inhibited the ability of CENPU to promote tumorigenesis in TNBC.

Collectively, the results of the present study indicated that CENPU promoted TNBC invasion, tumorigenesis and BCSC properties through the furin-proNGF-NGF signaling pathway. CENPU enhanced the conversion of proNGF to NGF by inhibiting furin degradation via the lysosomal pathway. However, there are certain limitations to the present study that warrant discussion. Two common strategies for enhancing enzyme activity were identified: Increasing the enzymatic affinity for its substrates and raising the enzymatic concentration. The present study demonstrated that the overexpression of CENPU could elevate furin activity. Both the substrate affinity of furin and its expression levels were examined, and it was observed that CENPU enhanced the activity and increased the expression of furin. However, while an increase in furin activity and expression levels was observed, the underlying molecular mechanisms that mediate these effects were not fully elucidated. Furthermore, a previous study has suggested that the activity of furin is regulated by its propeptide occupying the active site in its proenzyme form, thus preventing substrate binding (47). The present findings, however, indicate that CENPU may modulate furin activity through protein-protein interactions, which is not well-documented in the existing literature. Therefore, further research should be conducted to verify this hypothesis and explore the potential mechanisms.

In summary, the current findings revealed a novel mechanism underlying the tumor-promoting effect of CENPU, specifically in TNBC. The inhibition of CENPU expression and its downstream activated signaling pathway may be a novel strategy for TNBC treatment.

Acknowledgements

Not applicable.

Funding

The present study was supported by the Youth Natural Science Foundation of Shandong Province (grant nos. ZR2023QH128, ZR2023QH069 and ZR202211090247).

Availability of data and materials

The proteomics data generated in the present study may be found in the ProteomeXchange (iProX) repository under accession number PXD061628 or at the following URLs: https://www.iprox.cn/page/project.html?id=IPX0011300000 and http://proteomecentral.proteomexchange.org/cgi/GetDataset?ID=PXD061628. The other data generated in the present study may be requested from the corresponding author.

Authors' contributions

SS performed data collection, analysis and interpretation. ZH and LQ conducted data collection and analysis. DZ designed the study and supervised the data interpretation. SS and DZ confirm the authenticity of all the raw data. All authors have read and approved the final manuscript.

Ethics approval and consent to participate

The human and animal experiments in the present study were approved by the Ethics Committee of Shandong Cancer Hospital and Institute, Shandong First Medical University and Shandong Academy of Medical Sciences (approval nos. SDTHEC2022009017 and SDTHEC2022009018, respectively; Jinan, China). The human samples used in the present study were obtained with written informed consent from patients or their families (due to patient's physical reasons or low educational level) for use in research.

Patient consent for publication

Not applicable.

Competing interests

The authors declare that they have no competing interests.

References

1. Derakhshan F and Reis-Filho JS: Pathogenesis of triple-negative breast cancer. Annu Rev Pathol 17: 181-204, 2022.
2. Mahtani R, Kittaneh M, Kalinsky K, Mamounas E, Badve S, Vogel C, Lower E, Schwartzberg L and Pegram M; Breast Cancer Therapy Expert Group (BCTEG): Advances in therapeutic approaches for triple-negative breast cancer. Clin Breast Cancer 21: 383-390, 2021.

3. Zhang M, Deng H, Hu R, Chen F, Dong S, Zhang S, Guo W, Yang W and Chen W: Patterns and prognostic implications of distant metastasis in breast cancer based on SEER population data. Sci Rep 15: 26717, 2025.
4. Zhao S, Zuo WJ, Shao ZM and Jiang YZ: Molecular subtypes and precision treatment of triple-negative breast cancer. Ann Transl Med 8: 499, 2020.
5. Li Y, Zhan Z, Yin X, Fu S and Deng X: Targeted therapeutic strategies for triple-negative breast cancer. Front Oncol 11: 731535, 2021.
6. Bou Zerdan M, Ghorayeb T, Saliba F, Allam S, Bou Zerdan M, Yaghi M, Bilani N, Jaafar R and Nahleh Z: Triple negative breast cancer: Updates on classification and treatment in 2021. Cancers (Basel) 14: 1253, 2022.
7. Zhang R, Tu J and Liu S: Novel molecular regulators of breast cancer stem cell plasticity and heterogeneity. Semin Cancer Biol 82: 11-25, 2022.
8. Liu H, Song Y, Qiu H, Liu Y, Luo K, Yi Y, Jiang G, Lu M, Zhang Z, Yin J, *et al*: Downregulation of FOXO3a by DNMT1 promotes breast cancer stem cell properties and tumorigenesis. Cell Death Differ 27: 966-983, 2020.
9. Zhu K, Xie V and Huang S: Epigenetic regulation of cancer stem cell and tumorigenesis. Adv Cancer Res 148: 1-26, 2020.
10. Al-Hajj M, Wicha MS, Benito-Hernandez A, Morrison SJ and Clarke MF: Prospective identification of tumorigenic breast cancer cells. Proc Natl Acad Sci USA 100: 3983-3988, 2003.
11. Luo F, Zhang M, Sun B, Xu C, Yang Y, Zhang Y, Li S, Chen G, Chen C, Li Y and Feng H: LINC00115 promotes chemoresistant breast cancer stem-like cell stemness and metastasis through SETDB1/PLK3/HIF1α signaling. Mol Cancer 23: 60, 2024.
12. Lu H, Chen I, Shimoda LA, Park Y, Zhang C, Tran L, Zhang H and Semenza GL: Chemotherapy-induced Ca^{2+} release stimulates breast cancer stem cell enrichment. Cell Rep 18: 1946-1957, 2017.
13. Mannello F: Understanding breast cancer stem cell heterogeneity: Time to move on to a new research paradigm. BMC Med 11: 169, 2013.
14. Singh P, Pesenti ME, Maffini S, Carmignani S, Hedtfeld M, Petrovic A, Srinivasamani A, Bange T and Musacchio A: BUB1 and CENP-U, primed by CDK1, are the main PLK1 kinetochore receptors in mitosis. Mol Cell 81: 67-87.e9, 2021.
15. Pan T, Zhou D, Shi Z, Qiu Y, Zhou G, Liu J, Yang Q, Cao L and Zhang J: Centromere protein U (CENPU) enhances angiogenesis in triple-negative breast cancer by inhibiting ubiquitin-proteasomal degradation of COX-2. Cancer Lett 482: 102-111, 2020.
16. Lou Y, Lu J, Zhang Y, Gu P, Wang H, Qian F, Zhou W, Zhang W, Zhong H and Han B: The centromere-associated protein CENPU promotes cell proliferation, migration, and invasiveness in lung adenocarcinoma. Cancer Lett 532: 215599, 2022.
17. Bruno F, Arcuri D, Vozzo F, Malvaso A, Montesanto A and Maletta R: Expression and signaling pathways of nerve growth factor (NGF) and pro-NGF in breast cancer: A systematic review. Curr Oncol 29: 8103-8120, 2022.
18. Marsland M, Dowdell A, Jiang CC, Wilmott JS, Scolyer RA, Zhang XD, Hondermarck H and Faulkner S: Expression of NGF/proNGF and their receptors TrkA, $p75^{NTR}$ and sortilin in melanoma. Int J Mol Sci 23: 4260, 2022.
19. Morisse M, Bourhis T, Lévêque R, Guilbert M, Cicero J, Palma M, Chevalier D, le Bourhis X, Toillon RA and Mouawad F: Influence of EGF and pro-NGF on EGFR/SORTILIN interaction and clinical impact in head and neck squamous cell carcinoma. Front Oncol 13: 661775, 2023.
20. Bradshaw RA, Pundavela J, Biarc J, Chalkley RJ, Burlingame AL and Hondermarck H: NGF and ProNGF: Regulation of neuronal and neoplastic responses through receptor signaling. Adv Biol Regul 58: 16-27, 2015.
21. Marcinkiewicz M, Marcinkiewicz J, Chen A, Leclaire F, Chrétien M and Richardson P: Nerve growth factor and proprotein convertases furin and PC7 in transected sciatic nerves and in nerve segments cultured in conditioned media: Their presence in Schwann cells, macrophages, and smooth muscle cells. J Comp Neurol 403: 471-485, 1999.
22. Yan R, Yalinca H, Paoletti F, Gobbo F, Marchetti L, Kuzmanic A, Lamba D, Gervasio FL, Konarev PV, Cattaneo A and Pastore A: The structure of the pro-domain of mouse proNGF in contact with the NGF domain. Structure 27: 78-89.e3, 2019.
23. Thomas G: Furin at the cutting edge: From protein traffic to embryogenesis and disease. Nat Rev Mol Cell Biol 3: 753-766, 2002.
24. He Z, Khatib AM and Creemers JWM: The proprotein convertase furin in cancer: More than an oncogene. Oncogene 41: 1252-1262, 2022.
25. Regua AT, Aguayo NR, Jalboush SA, Doheny DL, Manore SG, Zhu D, Wong GL, Arrigo A, Wagner CJ, Yu Y, *et al*: TrkA interacts with and phosphorylates STAT3 to enhance gene transcription and promote breast cancer stem cells in triple-negative and HER2-enriched breast cancers. Cancers (Basel) 13: 2340, 2021.
26. Livak KJ and Schmittgen TD: Analysis of relative gene expression data using real-time quantitative PCR and the 2(-Delta Delta C(T)) method. Methods 25: 402-408, 2001.
27. Raninga PV, Zeng B, Moi D, Trethowan E, Saletta F, Venkat P, Mayoh C, D'Souza RCJ, Day BW, Shai-Hee T, *et al*: CBL0137 and NKG2A blockade: A novel immuno-oncology combination therapy for Myc-overexpressing triple-negative breast cancers. Oncogene 44: 893-908, 2025.
28. Tang X, Cromwell CR, Liu R, Godbout R, Hubbard BP, McMullen TPW and Brindley DN: Lipid phosphate phosphatase-2 promotes tumor growth through increased c-Myc expression. Theranostics 12: 5675-5690, 2022.
29. American Veterinary Medical Association. AVMA guidelines for the euthanasia of animals: 2020 edition. AVMA, Schaumburg, IL, 2020.
30. Yan Y, Zuo X and Wei D: Concise review: Emerging role of CD44 in cancer stem cells: A promising biomarker and therapeutic target. Stem Cells Transl Med 4: 1033-1043, 2015.
31. Namekawa T, Ikeda K, Horie-Inoue K, Suzuki T, Okamoto K, Ichikawa T, Yano A, Kawakami S and Inoue S: ALDH1A1 in patient-derived bladder cancer spheroids activates retinoic acid signaling leading to TUBB3 overexpression and tumor progression. Int J Cancer 146: 1099-1113, 2020.
32. Ghebeh H, Sleiman GM, Manogaran PS, Al-Mazrou A, Barhoush E, Al-Mohanna FH, Tulbah A, Al-Faqeeh K and Adra CN: Profiling of normal and malignant breast tissue show CD44high/CD24low phenotype as a predominant stem/progenitor marker when used in combination with Ep-CAM/CD49f markers. BMC Cancer 13: 289, 2013.
33. DA Cruz Paula A and Lopes C: Implications of different cancer stem cell phenotypes in breast cancer. Anticancer Res 37: 2173-2183, 2017.
34. Seidah NG, Benjannet S, Pareek S, Savaria D, Hamelin J, Goulet B, Laliberte J, Lazure C, Chrétien M and Murphy RA: Cellular processing of the nerve growth factor precursor by the mammalian pro-protein convertases. Biochem J 314: 951-960, 1996.
35. Deichmann U, Schuster S, Mazat JP and Cornish-Bowden A: Commemorating the 1913 michaelis-menten paper die kinetik der invertinwirkung: Three perspectives. FEBS J 281: 435-463, 2014.
36. Hanissian SH, Akbar U, Teng B, Janjetovic Z, Hoffmann A, Hitzler JK, Iscove N, Hamre K, Du X, Tong Y, *et al*: cDNA cloning and characterization of a novel gene encoding the MLF1-interacting protein MLF1IP. Oncogene 23: 3700-3707, 2004.
37. Goldberg AL: Protein degradation and protection against misfolded or damaged proteins. Nature 426: 895-899, 2003.
38. Lim KC, Tyler CM, Lim ST, Giuliano R and Federoff HJ: Proteolytic processing of proNGF is necessary for mature NGF regulated secretion from neurons. Biochem Biophys Res Commun 361: 599-604, 2007.
39. Hayakawa Y, Sakitani K, Konishi M, Asfaha S, Niikura R, Tomita H, Renz BW, Tailor Y, Macchini M, Middelhoff M, *et al*: Nerve growth factor promotes gastric tumorigenesis through aberrant cholinergic signaling. Cancer Cell 31: 21-34, 2017.
40. Tomellini E, Touil Y, Lagadec C, Julien S, Ostyn P, Zietal-Gelus N, Meignan S, Lengrand J, Adriaenssens E, Polakowska R and Le Bourhis X: Nerve growth factor and proNGF simultaneously promote symmetric self-renewal, quiescence, and epithelial to mesenchymal transition to enlarge the breast cancer stem cell compartment. Stem Cells 33: 342-353, 2015.
41. Rockwell NC, Krysan DJ, Komiyama T and Fuller RS: Precursor processing by kex2/furin proteases. Chem Rev 102: 4525-4548, 2002.
42. Chen C, Gupta P, Parashar D, Nair GG, George J, Geethadevi A, Wang W, Tsaih SW, Bradley W, Ramchandran R, *et al*: ERBB3-induced furin promotes the progression and metastasis of ovarian cancer via the IGF1R/STAT3 signaling axis. Oncogene 39: 2921-2933, 2020.

43. Zhou B and Gao S: Pan-cancer analysis of FURIN as a potential prognostic and immunological biomarker. Front Mol Biosci 8: 648402, 2021.
44. Ji S, Li S, Gao H, Wang J, Wang K, Nan W, Chen H and Hao Y: An AIEgen-based 'turn-on' probe for sensing cancer cells and tiny tumors with high furin expression. Biomater Sci 11: 2221-2229, 2023.
45. Chen M, Pan Y, Liu H, Ning F, Lu Q, Duan Y, Gan X, Lu S, Hou H, Zhang M, *et al*: Ezrin accelerates breast cancer liver metastasis through promoting furin-like convertase-mediated cleavage of Notch1. Cell Oncol (Dordr) 46: 571-587, 2023.
46. Liu Z, Gu X, Li Z, Shan S, Wu F and Ren T: Heterogeneous expression of ACE2, TMPRSS2, and FURIN at single-cell resolution in advanced non-small cell lung cancer. J Cancer Res Clin Oncol 149: 3563-3573, 2023.
47. Schaale D, Laspa Z, Balmes A, Sigle M, Dicenta-Baunach V, Hochuli R, Fu X, Serafimov K, Castor T, Harm T, *et al*: Hemin promotes platelet activation and plasma membrane disintegration regulated by the subtilisin-like proprotein convertase furin. FASEB J 38: e70155, 2024.